J|A|C|S
ARTICLES
Published on Web 01/12/2002

Structural Analysis of Metal Ion Ligation to Nucleotides and Nucleic Acids Using Pulsed EPR Spectroscopy

Charles G. Hoogstraten, Christopher V. Grant,[‡] Thomas E. Horton,[†,§] Victoria J. DeRose,[†] and R. David Britt*

Contribution from the Department of Chemistry, University of California at Davis, One Shields Avenue, Davis, California 95616, and Department of Chemistry, Texas A & M University, College Station, Texas 77842

Received May 17, 2001. Revised Manuscript Received August 8, 2001

Abstract: Metal ions play key structural and functional roles in many nucleic acid systems, particularly as required cofactors for many catalytic RNA molecules (ribozymes). We apply the pulsed EPR technologies of electron spin−echo envelope modulation and electron spin−echo-electron nuclear double resonance to the structural analysis of the paramagnetic metal ion Mn(II) bound to nucleotides and nucleic acids. We demonstrate that pulsed EPR, supplemented with specific isotope labeling, can characterize ligation to nucleotide base nitrogens, outer-sphere interactions with phosphate groups, distances to sites of specific ^{2}H atom labels, and the hydration level of the metal ion. These techniques allow a comprehensive structural analysis of the mononucleotide model system MnGMP. Spectra of phenylalanine-specific transfer RNA from budding yeast and of the hammerhead ribozyme demonstrate the applicability of the methods to larger, structured RNA systems. This suite of experiments opens the way to detailed structural characterization of specifically bound metal ions in a variety of ribozymes and other nucleic acids of biological interest.

Introduction

Because nucleic acids are polyanions, interactions with cations are central to their chemical and biological properties. Divalent metal ions often have particularly potent and specific effects on the structure and stability of folded RNA molecules.[1] For many highly structured RNA molecules, the secondary structure (i.e., Watson−Crick helices) forms in moderate concentrations of monovalent salt, but addition of divalent cations is necessary for formation of the globular tertiary structure.[2] Details of the roles played by bound metal ions in RNA structure have recently begun to emerge, including the way in which clusters of divalent ions may form a charge-neutralizing core around which large RNA tertiary structures can form[3] and the mechanism by which specific metal ion sites modulate the balance between RNA secondary and tertiary structure.[4] Most naturally occurring catalytic RNA molecules rely on metal ions for catalytic as well as structural purposes under normal conditions.[5,6] Thus, an understanding of the structural properties of metal ion−RNA complexes is critical to the unraveling of the mechanism of action of ribozymes and other functional RNAs.

It is useful to think of metal ions bound to RNA as falling into three approximate classes.[2,7] The first class arises due to the high negative charge of polynucleotides, which attracts poorly localized "atmospheric" cations in a nonspecific manner.[8] Second, in folded RNA structures, numerous phosphate groups in proximity may form pockets of highly negative electrostatic potential, in which hydrated metal ions may become localized without taking on specific RNA-derived inner-sphere ligands.[2] The substitution-inert ion hexammine Co(III) has recently found elegant use as a probe of such sites.[9] Finally, highly structured RNA molecules may form specific sites that replace one or more aqua ligands in the first coordination sphere of the bound ion with ligands from the RNA itself. The latter two classes can be usefully distinguished due to a greater specificity for one or a small number of ionic species in the case of partial dehydration.[7] Site bound ions are the primary targets of structural characterization of metal ion−RNA interactions, but the always-present

* To whom correspondence should be addressed.
† Texas A & M University.
‡ Current address: Department of Chemical Physics, Weizmann Institute of Science, Rehovot 76100, Israel.
§ Current address: Beckman Coulter, Inc., 4300 N. Harbor Boulevard, Fullerton, CA 92834-3100.

(1) (a) Saenger, W. *Principles of Nucleic Acid Structure*; Springer-Verlag: New York, 1984; pp 201−219. (b) Misra, V. K.; Draper, D. E. *Biopolymers* **1998**, *48*, 113−135.
(2) Tinoco, I., Jr.; Bustamante, C. *J. Mol. Biol.* **1999**, *293*, 271−281.
(3) Cate, J. H.; Hanna, R. L.; Doudna, J. A. *Nat. Struct. Biol.* **1997**, *4*, 553−558.
(4) (a) Wu, M.; Tinoco, I., Jr. *Proc. Natl. Acad. Sci. U.S.A.* **1998**, *95*, 11555−11560. (b) Silverman, S. K.; Zheng, M.; Wu, M.; Tinoco, I., Jr.; Cech, T. R. *RNA* **1999**, *5*, 1665−1674.
(5) (a) Pyle, A. M. In *Metal Ions in Biological Systems: Interactions of Metal Ions with Nucleotides, Nucleic Acids, and Their Constituents*; Sigel, A., Sigel, H., Eds.; Marcel Dekker: New York, 1996; Vol. 32, pp 480−520. (b) Feig, A. L.; Uhlenbeck, O. C. In *The RNA World*, 2nd ed.; Gesteland, R. F., Cech, T. R., Atkins, J. F., Eds.; Cold Spring Harbor Laboratory Press: Cold Spring Harbor, New York, 1999; pp 287−319.
(6) Doherty, E. A.; Doudna, J. A. *Annu. Rev. Biochem.* **2000**, *69*, 597−615.
(7) Laing, L. G.; Gluick, T. C.; Draper, D. E. *J. Mol. Biol.* **1994**, *237*, 577−589.
(8) Anderson, C. F.; Record, M. T., Jr. *Annu. Rev. Phys. Chem.* **1995**, *46*, 657−700.
(9) Kieft, J. S.; Tinoco, I., Jr. *Structure* **1997**, *5*, 713−721.

10.1021/ja0112238 CCC: $22.00

sea of nonspecifically bound ions must be carefully accounted for in the interpretation of experimental results.

Beginning with classic studies on tRNA systems,[10] a wide variety of biochemical and biophysical techniques has been brought to bear on metal ion sites in RNA. Bulk binding curves for cations may be analyzed using techniques sensitive to the metal ions themselves, such as equilibrium dialysis[11] or solution EPR,[12] or to the nucleic acid component, such as circular dichroism or ultraviolet melting.[13] Site-specific information on the nucleic acid may be obtained by observing the broadening of specific NMR resonances at substoichiometric levels of paramagnetic metal ions such as Mn^{2+}.[14−19] Such studies, although they locate Mn^{2+} binding sites within the molecular framework, generally give little direct information on the specific structure and ligation of the metal site. Although some information is available from fluorescence studies on lanthanide ions,[20] what is needed to complement the above techniques is a generally applicable, site-specific spectroscopic method for analyzing cation sites looking out from the metal ion itself, rather than looking in from the nucleic acid.

In this work, we report the use of the pulsed EPR techniques of electron spin−echo envelope modulation (ESEEM)[21] and electron spin−echo-electron nuclear double resonance (ESE-ENDOR)[22] to the analysis of metal ion sites in mononucleotides and RNA. By overcoming inhomogeneous line-broadening effects, spin−echo EPR techniques allow the measurement of weak hyperfine and quadrupole interactions and thus the analysis of paramagnetic metal ion interactions with magnetic nuclei of ligands and nearby regions of bound macromolecules.[23] Specifically, the information contained in ESEEM and ESE-ENDOR spectra includes the chemical identities of interacting atoms via the nuclear Larmor frequencies ν_n, as well as quantitation of the corresponding hyperfine coupling constants and (for nuclear spin $I > 1/2$) nuclear quadrupolar coupling constants e^2qQ and asymmetry parameters η. The ligand hyperfine coupling A is divided into a scalar or isotropic portion A_{iso}, which is related to the extent of spin delocalization onto the nucleus, and (for axial symmetry) a dipolar or anisotropic portion A_{dip}, which is directly related to the metal−nucleus distance in the point−dipole approximation. The form of the spectrum depends on the relative magnitudes and signs of ν_n, e^2qQ, A_{iso}, and A_{dip}.

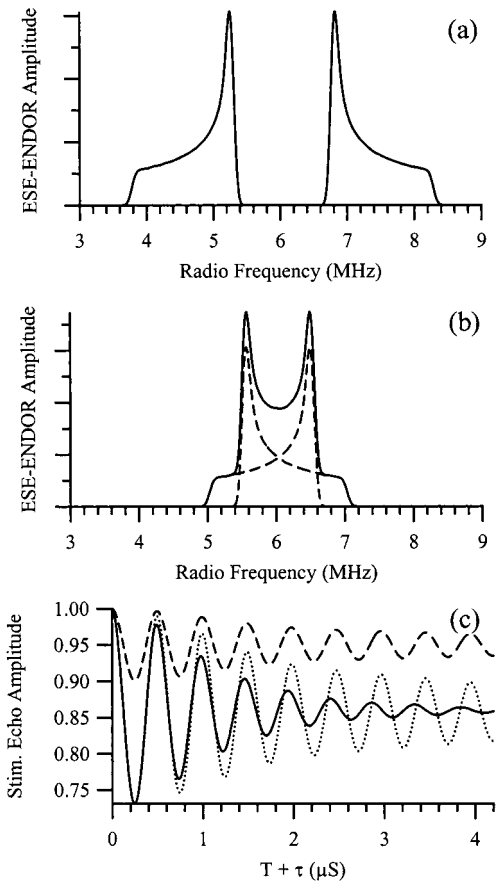

Figure 1. Illustrative simulated ESE-ENDOR and ESEEM data. (a) ^{31}P ENDOR powder pattern line shapes corresponding to an $S = I = 1/2$ system with an axially symmetric hyperfine interaction dominated by the scalar (isotropic) term. Simulation parameters: Microwave frequency, 10.2 GHz; static field strength, 3500 G; A_{iso}, 2.5 MHz; A_{dip}, 1.0 MHz (point−dipole distance, 3.2 Å); line shape convolved with Gaussian broadening function, half-width 15 kHz. (b) Same as (a) but with A_{iso} set to 0.0 for purely dipolar coupling. Individual powder pattern line shapes are shown as dashed lines. (c) Three-pulse ^2H ESEEM time-domain spectra for the $S = 1/2$, $I = 1$, weakly coupled case. Quadrupolar coupling e^2qQ, 0.22 MHz; asymmetry η, 0.1; ^2H resonance frequency, 2.0 MHz (3050 G); spin−echo delay τ, 251 ns; A_{iso}, 0.0 MHz. Dashed line: $A_{dip} = 0.26$ MHz (3.6 Å). Solid line: $A_{dip} = 0.45$ MHz (3.0 Å). Dotted line: cube of dashed line, corresponding to three equivalent ^2H atoms at 3.6 Å.

A combined analysis of ESEEM and ESE-ENDOR data can provide information on the number, type, and spatial distribution of magnetic nuclei in the neighborhood of the paramagnetic ion. For example, Figure 1a shows simulated ^{31}P ESE-ENDOR spectra for a phosphate group ligated in an inner-sphere fashion to Mn(II), a case in which the scalar coupling dominates. For such data, the scalar hyperfine coupling determines the distance between the centroids of the two ENDOR lines, whereas the width of each individual powder pattern line shape is controlled by the dipolar component. For more distant ^{31}P atoms, the scalar coupling will be negligible, and the two powder patterns will overlap, as shown in Figure 1b. In either case, a comparison of

(10) Schimmel, P. R.; Redfield, A. G. *Annu. Rev. Biophys. Bioeng.* **1980**, *9*, 181−221.
(11) (a) Schreier, A. A.; Schimmel, P. R. *J. Mol. Biol.* **1974**, *86*, 601−620. (b) Stein, A.; Crothers, D. M. *Biochemistry* **1976**, *15*, 157−160. (c) Bina-Stein, M.; Stein, A. *Biochemistry* **1976**, *15*, 3912−3917.
(12) Danchin, A.; Guéron, M. *Eur. J. Biochem.* **1970**, *16*, 532−536.
(13) (a) Cole, P. E.; Yang, S. K.; Crothers, D. M. *Biochemistry* **1972**, *11*, 4358−4368. (b) Puglisi, J. D.; Tinoco, I., Jr. *Methods Enzymol.* **1989**, *180*, 304−325.
(14) Bertini, I.; Luchinat, C. *NMR of Paramagnetic Molecules in Biological Systems*; Benjamin Cummings: Menlo Park, CA, 1986; pp 47−83.
(15) Marathias, V. M.; Wang, K. Y.; Kumar, S.; Pham, T. Q.; Swaminathan, S.; Bolton, P. H. *J. Mol. Biol.* **1996**, *260*, 378−394.
(16) (a) Chao, Y.-Y. H.; Kearns, D. R. *Biochim. Biophys. Acta* **1977**, *477*, 20−27. (b) Hurd, R. E.; Azhderian, E.; Reid, B. R. *Biochemistry* **1979**, *18*, 4012−4017. (c) Ott, G.; Arnold, L.; Limmer, S. *Nucleic Acids Res.* **1993**, *21*, 5859−5864.
(17) Hansen, M. R.; Simorre, J.-P.; Hanson, P.; Mokler, V.; Bellon, L.; Beigelman, L.; Pardi, A. *RNA* **1999**, *5*, 1099−1104.
(18) Butcher, S. E.; Allain, F. H.-T.; Feigon, J. *Biochemistry* **2000**, *39*, 2174−2182.
(19) Allain, F. H. T.; Varani, G. *Nucleic Acids Res.* **1995**, *23*, 341−350.
(20) (a) Draper, D. E. *Biophys. Chem.* **1985**, *21*, 91−101. (b) Feig, A. L.; Scott, W. G.; Uhlenbeck, O. C. *Science* **1998**, *279*, 81−84. (c) Feig, A. L.; Panek, M.; Horrocks, W. DeW., Jr.; Uhlenbeck, O. C. *Chem. Biol.* **1999**, *6*, 801−810.
(21) (a) Mims, W. B. In *Electron Paramagnetic Resonance*; Geschwind, S., Eds.; Plenum Press: New York, 1972; pp 263−351. (b) Mims, W. B.; Peisach, J. *Biol. Magn. Reson.* **1981**, *3*, 213−263. (c) Kevan, L. In *Time Domain Electron Spin Resonance*; Kevan, L., Schwartz, R. N., Eds.; Wiley-Interscience: New York, 1979; pp 279−341.
(22) (a) Hoffman, B. M.; DeRose, V. J.; Doan, P. E.; Gurbiel, R. J.; Houseman, A. L. P.; Telser, J. *Biol. Magn. Reson.* **1993**, *13*, 151−217. (b) Thomann, H.; Bernardo, M. *Biol. Magn. Reson.* **1993**, *13*, 275−322.
(23) Britt, R. D. In *Advances in Photosynthesis: Biophysical Techniques in Photosynthesis*; Hoff, A. J., Amesz, J., Eds.; Kluwer Academic Publishers: Amsterdam, 1995; pp 235−253.

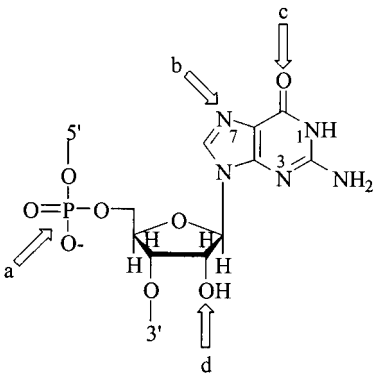

Figure 2. Available ion ligation groups in RNA. Chemical structure of a guanosine nucleotide residue within an RNA chain with possible ion ligation groups indicated. (a) Backbone phosphodiester oxygen; (b) aromatic ring nitrogen lone pair; (c) carbonyl oxygen; (d) 2′-hydroxyl oxygen.

experimental data with simulations provides both the scalar hyperfine coupling constant and the point−dipole Mn(II)−^{31}P distance.

For ESEEM experiments, by contrast, raw data are obtained in the time domain by varying timing parameters in two-pulse (primary echo) or three-pulse (stimulated echo) spin−echo sequences. Modulations in the echo intensity are observed at frequencies characteristic of hyperfine-coupled nuclei.[21] Usefully, the depth of modulations is related to the number of coupled nuclei, since the modulation pattern due to multiple coupled nuclei is simply the product of that expected from the individual couplings. ESEEM thus provides a method to count the number of atoms in a class of identically coupled nuclei, information difficult to obtain from ESE-ENDOR data. Figure 1c shows simulated time-domain ESEEM traces for single ^{2}H nuclei coupled to an electron spin-$^1/_2$ ion at two distinct distances as solid and dashed lines. These traces are easily distinguished by the depth of modulation. It can also be noted that, for the more distant nucleus (dashed line), the modulation decays more slowly with time in comparison to the closer nucleus (solid line). This effect arises because of the dispersion of modulation frequencies resulting from the greater anisotropic coupling in the latter case.[21a] Therefore, ESEEM modulation arising from several relatively distant nuclei can show initial modulation depth similar to that from a single nearby nucleus, but these two cases are cleanly distinguished by the differing time course of modulation decay (Figure 1c, solid and dotted traces).

Nucleotide residues in RNA and DNA contain a variety of potential metal ligands, including backbone phosphate groups, heterocyclic base nitrogen atoms, ring carbonyl groups, and (for RNA) 2′-hydroxyl groups (Figure 2). Outer-sphere, or water-mediated, ligation to nucleotide groups is also important owing to the tendency of metal ions bound to nucleic acids to retain a large fraction of their waters of hydration. Because of its high nucleophilicity, the N7 atom of guanosine is a particularly favorable ligand for Mn^{2+}.[1a,24] Phosphate and nitrogen ligation can be analyzed in natural isotopic abundance samples by measuring ^{31}P and ^{14}N hyperfine coupling interactions, respectively. Such data may be complemented by uniform or specific ^{15}N labeling. Examples of these interactions are given below. Analysis of carbonyl or 2′-hydroxyl ligation will require ^{13}C isotopic labeling and is deferred to another place.

In this report, using a complex of Mn^{2+} with guanosine 5′-monophosphate (MnGMP) as a model system, we derive a complete and consistent structural picture by analyzing interactions with ^{14}N, ^{15}N, ^{31}P, and ^{2}H nuclei of the nucleotide, as well as ^{2}H nuclei in ^2H_2O solvent. These experiments are shown to be easily generalizable to large RNA systems of biological interest, as is demonstrated using phenylalanine-specific transfer RNA (tRNA^{Phe}) from budding yeast. In a preliminary account of this work, we demonstrated the utility of ^{14}N and ^{15}N ESEEM to identify binding sites in a hammerhead ribozyme construct by comparison with MnGMP.[25]

Materials and Methods

All buffers, reagents, and nucleotides were purchased from Sigma at the highest purity available and were used without further purification, except as noted. GMP labeled with ^{15}N and ^{13}C was isolated from *E. coli* grown on labeled minimal medium[26] and was a kind gift of the laboratory of Dr. Thorsten Dieckmann. Labeled mononucleotide was desalted on a *cis*-boronate affinity column (Bio-Rad Affigel 601). The hammerhead ribozyme enzyme/substrate complex labeled with ^{15}N at all guanosine residues in the enzyme strand was prepared using in vitro transcription as previously described.[25] Guanosine 5′-monophosphate samples were 5 mM nucleotide, 1 mM $MnCl_2$ (unlabeled sample) or 2.5 mM nucleotide, 1 mM $MnCl_2$ (isotopically labeled sample). For all mononucleotide samples the only monovalent salt was that provided by the buffer, 10 mM sodium cacodylate at pH 7.0. GMP deuterated at the C8 carbon (GMP-d_1) was prepared by overnight treatment at 60 °C with 4 equiv of triethylamine in ^2H_2O.[27] Excess reagent was removed by repeated evaporation to dryness from ^1H_2O. Essentially complete exchange of H8 with negligible deuteration elsewhere was confirmed using ^{1}H NMR. The control sample for this study was treated in the same fashion as the GMP-d_1 except for the omission of the overnight base incubation. The yeast tRNA^{Phe} sample was 0.5 mM in tRNA, 0.2 mM in $MnCl_2$, 200 mM in NaCl, and 10 mM in sodium cacodylate buffer pH 7.0. GMP and tRNA samples were cryoprotected with 0.4 M sucrose prior to freezing and storage in liquid nitrogen.

Pulsed EPR spectroscopy was performed on a laboratory-built 8−18 GHz spectrometer previously described.[28] Two- and three-pulse ESEEM experiments were performed using standard methods[21,23] and Fourier-transformed using iterative reconstruction of the instrumental dead-time.[29] ESE-ENDOR spectra were collected using the method of Mims.[30] All spectroscopy was performed at 4.2 K. ESEEM simulations for the electron spin $S = {}^1/_2$, nuclear spin $I = {}^1/_2$ case were performed in the frequency domain according to the analytical expressions of Lai et al.[31] as implemented in Mathematica 3.0 (Wolfram Research). For the $I = 1$ case, simulations were performed in the time domain using numerical diagonalization of the spin Hamiltonian as described.[32] Time-domain simulations were apodized using a squared-cosine window and then Fourier-transformed to the frequency domain. ESE-ENDOR

(24) Streicher, B.; Wallis, M. G. In *Ribosomal RNA and Group I Introns*; Green, R., Schroeder, R., Eds.; R. G. Landes: Austin, TX, 1996; pp 103−128.
(25) Morrissey, S. R.; Horton, T. E.; Grant, C. V.; Hoogstraten, C. G.; Britt, R. D.; DeRose, V. J. *J. Am. Chem. Soc.* **1999**, *121*, 9215−9218.
(26) (a) Batey, R. T.; Inada, M.; Kujawinski, E.; Puglisi, J. D.; Williamson, J. R. *Nucleic Acids Res.* **1992**, *20*, 4515−4523. (b) Nikonowicz, E. P.; Sirr, A.; Legault, P.; Jucker, F. M.; Baer, L. M.; Pardi, A. *Nucleic Acids Res.* **1992**, *20*, 4507−4513.
(27) Huang, X.; Yu, P.; LeProust, E.; Gao, X. *Nucleic Acids Res.* **1997**, *25*, 4758−4763.
(28) (a) Sturgeon, B. E.; Britt, R. D. *Rev. Sci. Instrum.* **1992**, *63*, 2187−2192. (b)Sturgeon, B. E.; Ball, J. A.; Randall, D. W.; Britt, R. D. *J. Phys. Chem.* **1994**, *98*, 12871−12883.
(29) Mims, W. B. *J. Magn. Reson.* **1984**, *59*, 291−306.
(30) Mims, W. B. *Proc. R. Soc. London, Ser. A* **1965**, *283*, 452−457.
(31) Lai, A.; Flanagan, H. L.; Singel, D. J. *J. Chem. Phys.* **1988**, *89*, 7161−7166.
(32) Britt, R. D.; Zimmermann, J.-L.; Sauer, K.; Klein, M. P. *J. Am. Chem. Soc.* **1989**, *111*, 3522−3532.

simulations were performed using matrix diagonalization as described,[33] including the τ-dependent Mims suppression effect.[22]

Results

Directly Ligated ^{14}N and ^{15}N in Complexes of Mn(II) with GMP and the Hammerhead Ribozyme. In an earlier report, we used ^{14}N and ^{15}N ESEEM as a fingerprint for direct ligation of Mn(II) to aromatic ring nitrogens in GMP and the hammerhead ribozyme.[25] Here, we analyze this interaction in more detail using frequency-dependent ESEEM spectroscopy along with ^{15}N ESE-ENDOR. The combination of these techniques allows the extraction of the full hyperfine tensor for the interaction as well as the nuclear quadrupolar parameters for the ^{14}N ligand, yielding detailed information on the structure of the complex.

The desired hyperfine parameters can be most directly derived from observed ESE-ENDOR powder patterns for the nuclear spin $I = {}^1/_2$ case, corresponding to ^{15}N labeling of the nucleotide base. In our MnGMP samples, the GMP moiety is isotope-labeled with both ^{15}N and ^{13}C, and the interpretation of ^{15}N ESE-ENDOR at X-band is complicated by the presence of ^{13}C-derived powder patterns at overlapping frequencies (not shown). Therefore, we analyzed the powder patterns visible in the Mn−hammerhead ribozyme complex for which all guanosine residues on the ribozyme strand are ^{15}N-labeled,[25] and we applied the resulting parameters to the interpretation of further data in MnGMP. Under the conditions used (1 M NaCl), this hammerhead construct binds exactly one Mn(II) ion with high affinity.[34] This site has been studied extensively using EPR, phosphorothiate substitution, and NMR,[35] and the binding site was identified as a guanosine heterocycle nitrogen using ESEEM.[24] All features in the MnGMP ^{15}N ESE-ENDOR spectra which are resolved from ^{13}C patterns are identical to those in the ribozyme (not shown), as are those in ^{14}N and ^{15}N ESEEM, supporting the congruence of these two sites.

Figure 3 shows ESE-ENDOR spectra of the Mn(II)−hammerhead ribozyme complex collected using the method of Mims[30] at two different values of the static magnetic field, corresponding to two different maxima in the six-line Mn^{2+} EPR spectrum. For this case, the lower frequency (ν_-) ENDOR line occurs very close to zero frequency and is not observed. The data are fit well with an axially symmetric hyperfine coupling tensor with $A_{iso} = 4.2 \pm 0.1$ MHz and $A_{dip} = 0.9 \pm 0.1$ MHz and contributions from the central $S = \pm {}^1/_2$ spin manifold only. (As indicated, the analysis is complicated somewhat by the presence of a strong distant ^{23}Na peak). If it is assumed that A_{dip} arises only from dipole−dipole interactions, this result corresponds to a point−dipole distance between the Mn(II) ion and the interacting ^{15}N of 2.1 ± 0.1 Å, representing a direct, inner-sphere ligation of the ring nitrogen to the Mn(II) ion. Although this distance estimate will not be quantitatively accurate due to violations of the point−dipole approximation and nondipole−dipole contributions to the anisotropic hyperfine,

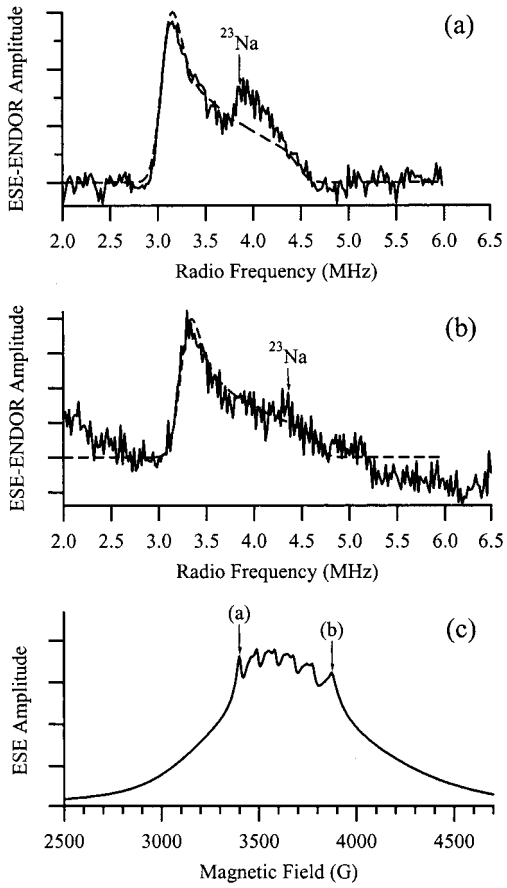

Figure 3. ^{15}N ESE-ENDOR of Mn(II) bound to the hammerhead ribozyme. Mims ESE-ENDOR spectra for a complex of Mn(II) with a hammerhead ribozyme construct labeled with ^{15}N at guanosine residues in the "ribozyme" strand.[25] Data were acquired at X-band (10.3 MHz) with a spin−echo delay τ of 120 ns and static magnetic fields of (a) 3430 G and (b) 3870 G. Corresponding simulations using $A_{iso} = 4.2$ MHz and $A_{dip} = 0.9$ MHz are shown with dashed lines. Simulations were convolved with a Gaussian line shape ($a = 40$ kHz) to represent line-broadening effects. (c) Field-swept ESE-EPR spectrum of the Mn(II)−hammerhead sample with the fields used for ENDOR data acquisition indicated.

the data are clearly sufficient to distinguish direct coordination of ^{15}N from outer-sphere or indirect interactions.

The ^{15}N hyperfine tensor determined above implies that, at X-band frequencies of ca. 9−10 GHz, molecules at a subset of orientations with respect to the static magnetic field will fulfill the "exact cancellation" condition $A/2 \approx \nu_n$, where ν_n is the nuclear Larmor frequency, with consequent dramatic enhancement of ESEEM modulation for both ^{15}N and ^{14}N.[31,36] These effects are visible in the X- and P-band ESEEM spectra for ^{15}N−MnGMP shown in Figure 4a and b. Simulations performed with the analytical formalism of Singel and co-workers[31] using the hyperfine values derived from ESE-ENDOR reproduce the data quite well overall. We note that the predicted sharpening at the lower-frequency edge of the X-band ESEEM line shapes, which intensifies to a near singularity at 3890 G corresponding to the precise exact-cancellation condition, is not fully observed, presumably due to a distribution in hyperfine constants, slight hyperfine rhombicity, or other effects. The general agreement between predicted and observed line shapes over a wide

(33) Randall, D. W.; Sturgeon, B. E.; Ball, J. A.; Lorigan, G. A.; Chan, M. K.; Klein, M. P.; Armstrong, W. H.; Britt, R. D. *J. Am. Chem. Soc.* **1995**, *117*, 11780−11789.
(34) Horton, T. E.; Clardy, D. R.; DeRose, V. J. *Biochemistry* **1998**, *37*, 18094−18101.
(35) (a) Morrissey, S. R.; Horton, T. E.; DeRose, V. J. *J. Am. Chem. Soc.* **2000**, *122*, 3473−3481. (b) Hunsicker, L. M.; DeRose, V. J. *J. Inorg. Biochem.* **2000**, *80*, 271−281. (c) Maderia, M.; Hunsicker, L. M.; DeRose, V. J. *Biochemistry* **2000**, *39*, 12113−12120.
(36) (a) Mims, W. B.; Peisach, J. *J. Chem. Phys.* **1978**, *69*, 4921−4930. (b) Flanagan, H. L.; Singel, D. J. *J. Chem. Phys.* **1987**, *87*, 5606−5616.

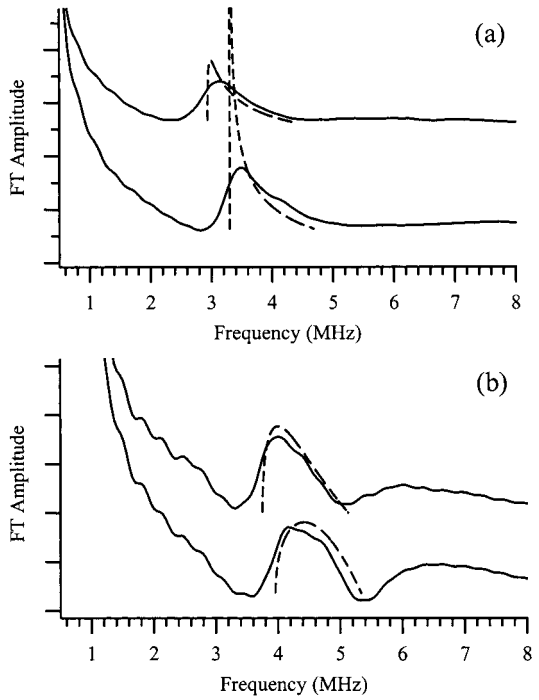

Figure 4. Multifrequency ^{15}N ESEEM of MnGMP. Fourier-transformed two-pulse ESEEM spectra at 9.2 GHz (a) and 14.5 GHz (b) for a ^{15}N,^{13}C-MnGMP sample. Two independent field values (maxima in the six-line Mn(II) EPR line shape) are shown for each frequency band. Simulations according to the formalism of Singel and co-workers[31] using parameters derived from ESE-ENDOR data in Figure 3 are shown as dashed lines. Within each panel, the two experimental traces and the two theoretical traces are on the same scale, but the vertical scale between data and simulations is arbitrary.

frequency range, however, increases our confidence in the hyperfine values reported above.

Scaling the above results by the respective gyromagnetic ratios predicts a hyperfine tensor for the Mn(II)−^{14}N interaction in MnGMP with $A_{iso} = 3.0$ MHz and $A_{dip} = 0.6$ MHz. The ^{14}N ESEEM patterns will also be affected by the nuclear quadrupolar tensor for the spin-1 ^{14}N nucleus. For an $S = {}^1/_2$, $I = 1$ spin system with purely isotropic hyperfine coupling near the exact cancellation condition, the Fourier-transformed ESEEM spectrum is characterized by three sharp lines whose frequencies uniquely define the quadrupolar parameters e^2qQ and η for the spin-1 nucleus, along with a "double-quantum" peak arising from the noncanceled electron spin manifold at higher frequency.[36] ^{14}N ESEEM has been performed for Mn(II) bound to imidazole moieties in several systems, and frequency-domain spectra substantially more complex than the simple four-line exact cancellation picture have been observed.[37] This added complexity is attributed to anisotropic contributions to the hyperfine tensor and/or contributions from the outer electron spin manifolds of $S = {}^5/_2$ Mn(II). For ligation of Mn(II) to the imidazole-like nitrogen of a guanosine ring, we have attempted to simulate the ^{14}N ESEEM patterns using an algorithm that takes both isotropic and anisotropic hyperfine interactions into account, albeit neglecting nonspin-$^1/_2$ effects.[32]

In Figure 5 we show X- and P-band ^{14}N ESEEM spectra for the MnGMP complex (left), along with simulations calculated using hyperfine constants derived from ^{15}N ENDOR data and $e^2qQ = 3.2$ MHz, $\eta = 0.30$ (center), and simulations with $A_{iso} = 2.1$ MHz, $A_{dip} = 0.4$ MHz, $e^2qQ = 2.9$ MHz, $\eta = 0.40$ (right). The choice of quadrupolar parameters in these simulations was largely made to achieve agreement with low-frequency resonances at P-band. The requirement that the hyperfine tensor components agree with those predicted from ^{15}N ESE-ENDOR (Figure 5b,e,h) reproduces many features of the experimental spectrum, particularly at P-band frequencies. Serious discrepancies remain, however, most notably in the X-band "double quantum" peak, which is consistently too high by 1 MHz or more. Relaxing this condition and reducing the hyperfine components improves the situation somewhat (Figure 5c,f,i), although the detailed agreement at low nuclear frequencies is still poor, and varying the hyperfine tensor upon isotopic substitution is poorly justified. Many of the experimental features that we have not successfully simulated may well arise from outer electron spin manifolds (nonspin-$^1/_2$ effects). Substantial changes in the form of the spectra can also be seen if the angle between the principal axes of the quadrupolar and hyperfine tensors is varied;[38] we did not take this effect into account here. In Figure 6, we show two-pulse ESEEM data for MnGMP collected across the ESE-EPR spectral envelope, including the broad wings which are dominated by the noncentral manifolds. The diminution and shift of ESEEM frequencies at these wings support both the assignment of the major transitions to the central manifolds and the contribution of $S = {}^5/_2$ effects to fine details of the spectra. Fully rigorous ESEEM simulations for the $S = {}^5/_2$, $I = 1$ case are nontrivial and are deferred to another place. The current analysis, however, does give chemically useful estimates of the quadrupolar parameters (see Discussion). In summary, the combination of ESEEM and ESE-ENDOR for both ^{14}N and ^{15}N systems has allowed improved analysis of the parameters relating to the molecular structure of Mn−N ligation in this complex relative to ^{14}N ESEEM alone, although some ambiguities remain.

Site Identification Using Deuterium Labeling. The covalent structure of GMP (Figure 2) contains several chemically similar aromatic ring nitrogen atoms, any one of which could give rise to data such as that in Figures 3−6 if directly ligated to Mn(II). Although the N7 site is the most plausible ligand on chemical grounds,[1a,24] we desired a direct experimental determination of the precise site of ion ligation. We therefore performed ^{2}H ESEEM on a complex of Mn(II) with GMP labeled with ^{2}H at the H8 position (MnGMP-d_1), analyzing the results by comparison with the known Mn(II)−^{2}H distance in MnEDTA.[39] As described in the Supporting Information, this procedure gave a value of 3.6 ± 0.1 Å for the Mn(II)−^{2}H distance, consistent with ligation to the N7 but not the N3 of the nucleotide. Site-specific isotope labeling in combination with ESEEM allowed an unambiguous determination of the exact site of metal ligation. In agreement with the ESEEM data, ^{1}H CW-ENDOR of MnGMP-d_1 previously revealed the loss of a signal with 1.7 MHz splitting as compared to that of unlabeled MnGMP.[35a]

(37) (a) McCracken, J.; Peisach, J.; Bhattacharyya, L.; Brewer, F. *Biochemistry* **1991**, *30*, 4486-4491. (b) Espe, M. P.; Hosler, J. P.; Ferguson-Miller, S.; Babcock, G. T.; McCracken, J. *Biochemistry* **1995**, *34*, 7593−7602. (c) Buy, C.; Girault, G.; Zimmermann, J.-L. *Biochemistry* **1996**, *35*, 9880−9891. (d) Lee, H. C.; Goroncy, A. K.; Peisach, J.; Cavada, B. S.; Grangeiro, T. B.; Ramos, M. V.; Sampaio, A. H.; Dam, T. K.; Brewer, C. F. *Biochemistry* **2000**, *39*, 2340−2346.

(38) Reijerse, E. J.; Keijzers, C. P. *J. Magn. Reson.* **1987**, *71*, 83−96.

(39) de Beer, R.; de Boer, W.; van't Hof, C. A.; van Ormondt, D. *Acta Crystallogr.* **1973**, *B29*, 1473−1480.

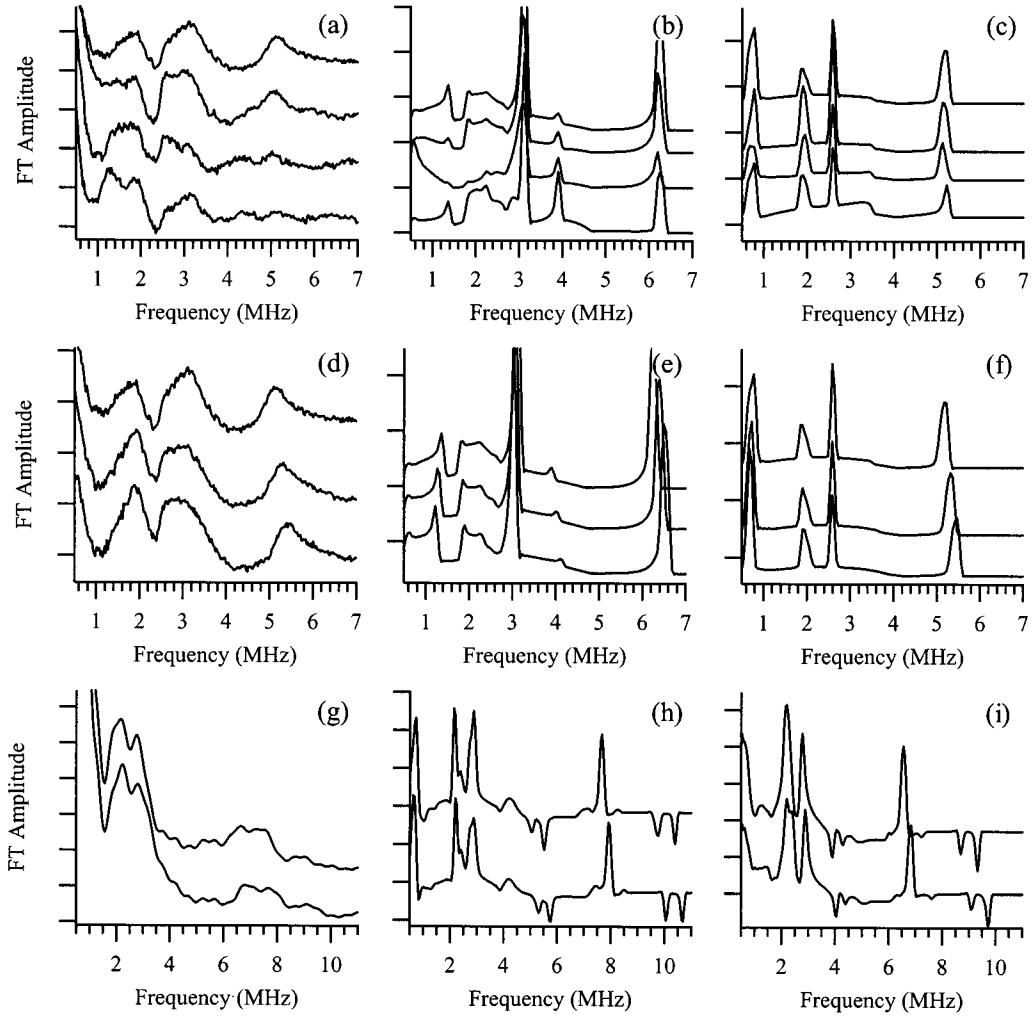

Figure 5. Multifrequency ^{14}N ESEEM of MnGMP. Comparison of experimental (left) and simulated (center, right) ESEEM of natural isotopic-abundance MnGMP. (a,b,c) X-band (10.2 GHZ, 3420 G) three-pulse ESEEM, comparison of spin−echo delays τ. Top to bottom, τ = 206, 275, 343, 550 ns. (d,e,f) Three-pulse ESEEM at 10.2 GHZ acquired at magnetic fields corresponding to three different maxima of the Mn(II) EPR spectrum. Top to bottom, 3420 G and 206 ns τ, 3670 G and 192 ns, 3890 G and 181 ns. (g,h,i) P-band (17.1 GHz) two-pulse ESEEM at fields of 5880 G (top) and 6350 G (bottom). Simulations for corresponding experimental parameters were performed for an $S = {}^1/_2$, $I = 1$ spin system[32] with collinear hyperfine and quadrupolar tensors and parameters of (b,e,h) $A_{iso} = 3.0$ MHz, $A_{dip} = 0.65$ MHz, $e^2qQ = 3.2$ MHz, $\eta = 0.30$; or (c,f,i) $A_{iso} = 2.1$ MHz, $A_{dip} = 0.40$ MHz, $e^2qQ = 2.9$ MHz, $\eta = 0.4$.

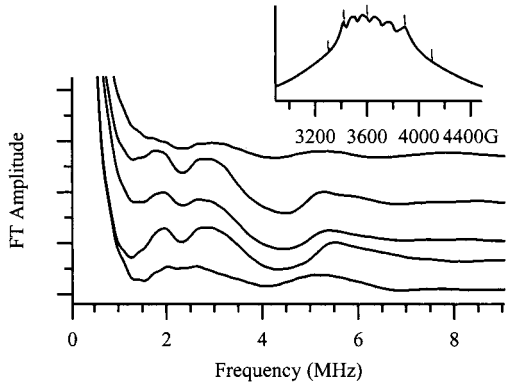

Figure 6. Field dependence of ESEEM modulation in MnGMP. Two-pulse ESEEM spectra at X-band (10.2 GHZ). Magnetic fields, top to bottom, are 3300, 3420, 3600, 3890, and 4100 G. The inset indicates the fields used on the ESE-EPR field-swept spectral envelope.

Analysis of Outer-Sphere Phosphate Ligands Using ESE-ENDOR. ESEEM spectroscopy has been used to analyze Mn^{2+}-phosphate ester ligation at the active sites of a variety of enzyme systems involving nucleotide cofactors,[37c,40] and we have detected strongly coupled ^{31}P interactions using ESE-ENDOR in mononucleotide complexes including MnATP (C.G.H., C.V.G., and R.D.B., data not shown). The MnGMP complex shows no evidence for such inner-sphere interactions. With the use of long spin−echo delays τ, however, the Mims ESE-ENDOR sequence can be optimized for the detection of magnetic nuclei at relatively long distances. For aqueous solutions of nucleic acids, such interactions correspond to "outer-sphere" or water-mediated contacts with groups including ^{31}P in phosphate. Experimental data and simulations for 600 and 1000 ns τ Mims ENDOR in MnGMP are shown in Figure 8. We assume that the observed line shape arises exclusively from the central $M_S = -{}^1/_2 \leftrightarrow M_S = +{}^1/_2$ EPR transition; this interpretation is supported by the lack of ENDOR observed when the magnetic field is set in the wings of the EPR spectrum, where the outer transitions dominate (Figure 7b,c). For this

(40) (a) LoBrutto, R.; Smithers, G. W.; Reed, G. H.; Orme-Johnson, W. H.; Tan, S. L.; Leigh, J. S., Jr. *Biochemistry* **1986**, *25*, 5654−5660. (b) Tipton, P. A.; McCracken, J.; Cornelius, J. B.; Peisach, J. *Biochemistry* **1989**, *28*, 8, 5720−5728. (c) Larsen, R. G.; Halkides, C. J.; Redfield, A. G.; Singel, D. J. *J. Am. Chem. Soc.* **1992**, *114*, 9608−9611.

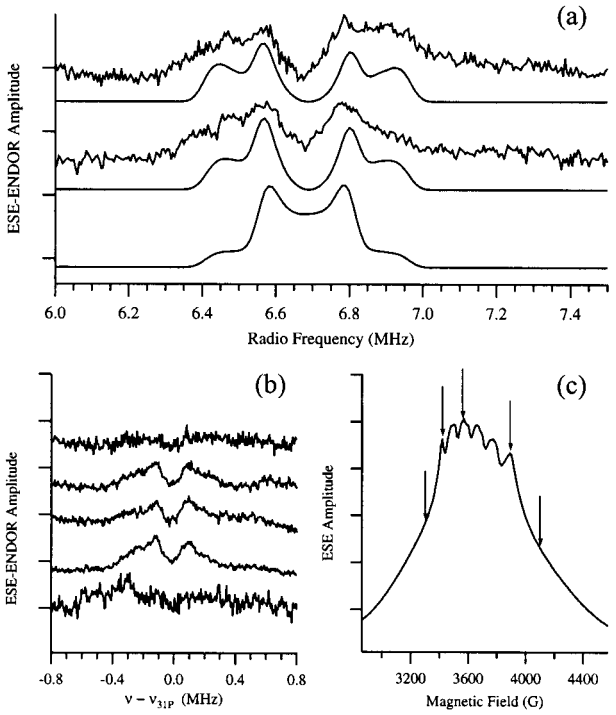

Figure 7. Demonstration of outer-sphere ^{31}P ligation in MnGMP using ESE-ENDOR. (a) Mims ESE-ENDOR of MnGMP with spin−echo delays τ of (top) 600 ns, (middle) 1000 ns. Simulations including the τ-dependent suppression effect and using $A_{iso} = 0.08$ MHz, $A_{dip} = 0.31$ MHz accompany the data traces; reconstructed suppressionless powder pattern is at bottom (cf. Figure 1b). Spectra acquired at 3880 G, 10.2 GHz, RF pulse width 16 μs. (b) ^{31}P ESE-ENDOR spectra of MnGMP as a function of magnetic field, increasing field from top to bottom; fields used are shown on the Mn(II) ESE-EPR spectrum in (c).

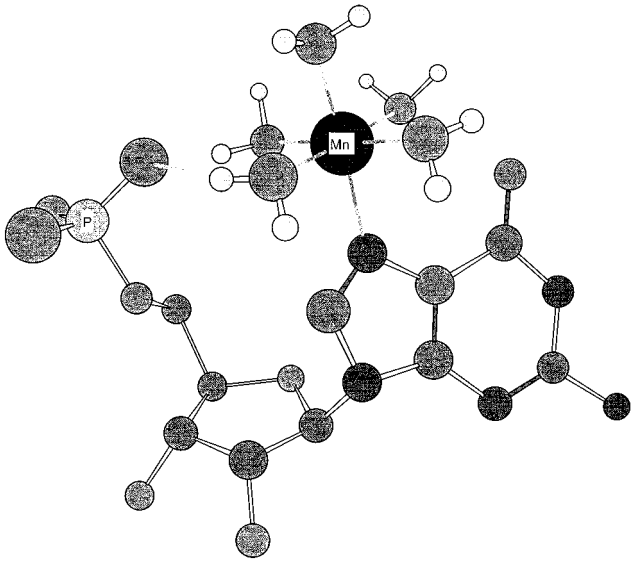

Figure 8. Molecular model of the $Mn(H_2O)_5$−GMP complex consistent with ESEEM and ESE-ENDOR data. Hydrogen atoms on the GMP moiety are omitted for clarity. Figure was prepared with Chem3D (Cambridge Scientific Computing).

interaction, essentially no electron delocalization onto the ^{31}P is seen ($A_{iso} \approx 0$), and a dipolar coupling A_{dip} corresponding to a point−dipole distance of 5.0 ± 0.4 Å is obtained. This distance is compatible with the range of metal−phosphorus distances observed for water-mediated phosphate ligation in a survey of high-resolution RNA crystal structures deposited in the Nucleic Acid Databank (not shown). The ENDOR data thus indicate an outer-sphere macrochelate interaction in the MnGMP complex, with the Mn^{2+} ion ligated directly to the base N7 and indirectly via a water of hydration to a phosphate oxygen (Figure 8).

Quantitation of Metal Ion Hydration in MnGMP Using ESEEM. The extent to which hexaquo Mn(II) is dehydrated upon nucleic acid or nucleotide ligation plays a key role in the energetics and specificity of the binding process.[1] Experimental methods for addressing this parameter in a particular structure, however, are sparse, the best-developed being a fluorescence lifetime measurement applicable only to lanthanides such as Tb(III) and Eu(III).[20] Since ESEEM is capable of quantitating the number of identical magnetic nuclei coupled to an electron spin and can give signals from ^{1}H and ^{2}H atoms in solvent water, it has the potential to overcome this limitation.[41] We have developed a robust and precise methodology to count the number of first-sphere aqua ligands to Mn(II) ions bound to nucleotides and nucleic acids using ^{2}H ESEEM.[42] Application of this procedure to the MnGMP case (see Supporting Information) yielded a count of 5.2 ± 0.1 aqua ligands to the Mn(II). These results are consistent with the analysis of this complex reported above, in which one inner-sphere ligand, the ring N7, is derived from the nucleotide itself (Figure 8), implying an octahedral, pentahydrate Mn(II).

Analysis of a Unique Mn^{2+} Site in Yeast $tRNA^{Phe}$. Phenylalanine-specific transfer RNA ($tRNA^{Phe}$) from the budding yeast *Saccharomyces cerevisiae* has become a paradigmatic system for both structure and metal binding in RNA systems by virtue of the vast amount of structural and biophysical data available.[10−13,16,20a] Crystallographic studies in Mg^{2+} have found a small number of metal binding sites to be consistently filled.[43] In crystals of yeast $tRNA^{Phe}$ soaked with Mn^{2+}, a single bound Mn^{2+} ion which had one inner-sphere RNA-derived ligand, the N7 of guanosine 20, was found.[44] A variety of solution techniques have found tRNA to bind a number of metal ions in cooperative fashion under low-salt conditions;[6,10] however, at 150−200 mM NaCl, $tRNA^{Phe}$ was found by solution EPR to bind one or at most two Mn^{2+} ions with high affinity.[45] We therefore chose this tRNA molecule at moderate salt concentrations as an initial test of pulsed EPR's ability to analyze specific metal sites in relatively large RNA systems.

Figure 9 shows ESEEM and ESE-ENDOR results for our sample of yeast $tRNA^{Phe}$ in 200 mM NaCl. Two-pulse ESEEM clearly demonstrates the presence of a ring nitrogen ligand with similar hyperfine and quadrupolar parameters to those observed in MnGMP. Again, as for MnGMP, no evidence for strongly coupled (i.e., inner-sphere) phosphate ligands was found. However, long-τ Mims ENDOR does reveal a powder pattern similar to, although somewhat less resolved than, that shown in Figure 7 for MnGMP (Figure 9b). The apparent point−dipole distance of 4.9 Å is again consistent with a water-mediated hydrogen bond interaction with at least one phosphate group.

(41) Serpersu, E. H.; McCracken, J.; Peisach, J.; Mildvan, A. S. *Biochemistry* **1988**, *27*, 8034−8044.
(42) Hoogstraten, C. G.; Britt, R. D. *RNA*. In press.
(43) (a) Holbrook, S. R.; Sussman, J. L.; Warrant, R. W.; Church, G. M.; Kim, S.-H. *Nucleic Acids Res.* **1977**, *4*, 2811−2820. (b) Quigley, G. J.; Teeter, M. M.; Rich, A. *Proc. Natl. Acad. Sci. U.S.A.* **1978**, *75*, 64−68.
(44) Jack, A.; Ladner, J. E.; Rhodes, D.; Brown, R. S.; Klug, A. *J. Mol. Biol.* **1977**, *111*, 315−328.
(45) Leroy, J. L.; Guéron, M. *Biopolymers* **1977**, *16*, 2429−2446.

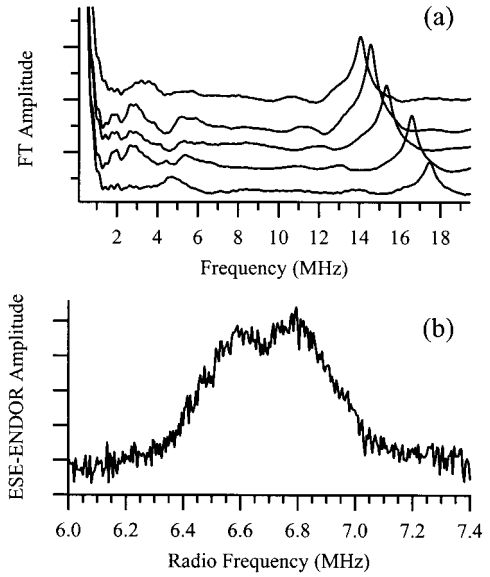

Figure 9. Pulsed EPR data on Mn(II) bound to yeast $tRNA^{Phe}$. (a) Two-pulse ESEEM at 10.2 GHz. Magnetic fields, top to bottom: 3300, 3416, 3600, 3892, 4100 G. The highest and lowest field correspond to the poorly resolved shoulders of the Mn(II) ESE-EPR line shape. (b) ^{31}P long-range ESE-ENDOR at 3890 G, $\tau = 600$ ns, 10.2 GHz, 16 μs RF pulse.

Intensity within ± 0.1 MHz of the ^{31}P Larmor frequency presumably arises from numerous long-range interactions with a subset of the 70 or more ^{31}P atoms in the tRNA that are not in the first or second coordination spheres of the ligated Mn(II). The ligation pattern revealed is consistent with that observed crystallographically for Mn^{2+} by Jack et al.,[44] although the EPR data do not distinguish the particular binding pocket of tRNA occupied under our solution conditions (see below).

Discussion

In this work, we used the MnGMP metal−nucleotide complex as a model system to explore the structural analysis possible in complexes of divalent ions with RNA and DNA using pulsed EPR spectroscopy. We find the environment of Mn(II) in MnGMP to consist of inner-sphere ligation to N7 of the guanine ring, outer-sphere water-mediated ligation to the GMP phosphate group, and the retention of five of the original six aqua ligands in the first coordination sphere (Figure 7). The independent determination of the number of H_2O ligands (Supporting Information), which yields a result fully consistent with results based on identification of nucleotide-derived ligands, provides an extremely valuable cross-check among the various data. Interestingly, our solution results yield the exact conformation of this complex found to exist in the crystal state.[46] Our data are also consistent with the thermodynamic analysis of Sigel and co-workers, who found evidence for a substantial degree of macrochelate formation in solution.[47] Since the potentiometric titration data reported for the MnGMP complex provided precise thermodynamic parameters but only indirect evidence for the nature of the important interactions (i.e., inner-sphere vs outer-sphere), the structural results derived with pulsed EPR provide an excellent complement to such an analysis.

As expected from the chemical similarity of the systems, ^{14}N ESEEM spectra in MnGMP closely resemble spectra previously obtained for Mn(II) bound to imidazole rings, including histidine side chains in proteins.[37] In our case, the availability of directly comparable ^{15}N ESE-ENDOR data has provided an independent determination of the hyperfine tensor for the Mn(II)−^{14}N interaction. Detailed simulations of ESEEM data using these values have allowed useful estimates of e^2qQ and η to be derived, although some ambiguity remains due to neglect of possible tensor noncollinearity and outer-manifold effects for the $S = {}^5/_2$ Mn(II) ion.

The derived values of $e^2qQ = 3.2$ MHz and $\eta = 0.30$ are chemically reasonable for the N7 atom of the MnGMP system. These parameters were measured using quadrupole double resonance as 3.26 and 0.16 MHz, respectively, in free guanine.[48] Although direct measurements of quadrupolar parameters for MnGMP are not available, the effect of metal ligation to imidazole and derivatives has been studied.[49] In general, metal ligation to imino nitrogens was found to decrease e^2qQ and increase η, in accord with the differences between our results and the NQR parameters for free guanine. Indeed, our parameters fall on the linear anticorrelation between e^2qQ and η for free nucleosides noted by Garcia and Smith[48] and attributed to the dominant effect of changes in 2p orbital electron density with the q_{zz} axis of the electric field gradient tensor located along the nitrogen lone-pair orbital. Thus, the parameters used to simulate the ^{14}N ESEEM in Figure 5 (b,e,h) are consistent with our understanding of chemical structure in metal complexes with aromatic heterocycles.

In most cases, the physiological divalent ion bound to DNA or RNA in the cell is presumed to be Mg^{2+}, which is relatively silent spectroscopically (see, however, ref 50). Replacement with the paramagnetic probe ion Mn^{2+}, however, carries the potential risk of perturbing the interactions of interest. Nevertheless, in terms of ionic radius, coordination geometry, and ligand preferences, Mn^{2+} is a good mimic of Mg^{2+} in solution, although with a somewhat increased preference for soft ligands such as N and S.[51] Mn^{2+} is also the only ion that can fully replace Mg^{2+} for the large, complex group I intron and RNase P ribozymes, which otherwise show substantial selectivity in their ionic cofactors.[5] Thus, in many cases of interest, Mn(II) will be a relatively nonperturbing substitution for Mg^{2+}.

A critical element in applying the methods demonstrated here to the variety of biologically interesting metal−nucleic acid complexes[1−6] is generalization to RNA molecules of arbitrary size. As a solid-state technique, pulsed EPR does not suffer from the degradation of resolution observed in solution NMR as molecular size increases, and applications to large multiprotein complexes are routine.[23] To demonstrate this advantage in nucleic acids, we chose the paradigmatic system of yeast $tRNA^{Phe}$, whose metal-binding properties have been the subject of detailed interdisciplinary study.[10−13] Under the ionic condi-

(46) de Meester, P.; Goodgame, D. M. L.; Jones, T. J.; Skapski, A. C. *Biochem. J. (London)* **1974**, *139*, 791−792.
(47) Sigel, H.; Massoud, S. S.; Corfù, N. A. *J. Am. Chem. Soc.* **1994**, *116*, 2958−2971.
(48) Garcia, M. L. S.; Smith, J. A. S. *J. Chem. Soc., Perkin Trans. 2* **1983**, 1401−1408.
(49) Ashby, C. I. H.; Cheng, C. P.; Brown, T. L. *J. Am. Chem. Soc.* **1978**, *100*, 6057−6063.
(50) Grant, C. V.; Frydman, V.; Frydman, L. *J. Am. Chem. Soc.* **2000**, *122*, 11743−11744.
(51) (a) Bock, C. W.; Katz, A. K.; Markham, G. D.; Glusker, J. P. *J. Am. Chem. Soc.* **1999**, *121*, 7360−7372. (b) Reed, G. H.; Poyner, R. R. In *Metal Ions in Biological Systems: Manganese and its Role in Biological Processes*; Sigel, A., Sigel, H., Eds.; Marcel Dekker: New York, 2000; Vol. 37, pp 183−207.

tions used here, $tRNA^{Phe}$ binds 1−2 Mn^{2+} ions with strong affinity.[45] The picture of Mn(II) as binding to $tRNA^{Phe}$ with a single nitrogenous ligand is consistent with an early study of Mn^{2+} soaking into $tRNA^{Phe}$ crystals, which found a single Mn^{2+} bound through the N7 atom of G20.[44] A recent refinement of the $tRNA^{Phe}$ structure found a different geometry for the most highly occupied Mn^{2+} site, however.[52] In any case, the pulsed EPR data alone do not identify the region on the tRNA three-dimensional structure in which Mn(II) is bound. Complementary paramagnetic NMR broadening[14−19] or specific isotope labeling[25] studies will be necessary to resolve this issue for a particular system.

The interpretation of pulsed EPR data is unambiguous only when the ion analyzed is in a single, homogeneous environment at a unique site on the nucleotide or nucleic acid. For mononucleotides, this may be achieved by using a sufficient excess of ligand. For our 5 mM GMP, 1 mM Mn^{2+} samples, for example, a log K_M^M value of 2.39 measured at 0.1 M salt predicts greater than 50% of Mn(II) to exist in bound form;[47] at the low salt conditions used here, this number will presumably be increased due to the substantial electrostatic component to binding. Indeed, we observe a dramatic decrease of ^{14}N ESEEM modulation in 0.2 M NaCl as compared to the conditions used above (data not shown). In the case of $tRNA^{Phe}$, we have chosen ionic conditions at which solution EPR data indicate 1−2 strongly bound Mn^{2+} ions.[45] The significance of these and other metal-binding data in tRNA has been questioned, with the concept of "strong" versus "weak" sites criticized as an artifact of global electrostatic effects.[53] In a recent careful study, Misra and Draper were able to reproduce Mg^{2+}-binding data to tRNA at up to 32 mM salt using a nonlinear Poisson−Boltzmann electrostatic model with no adjustable parameters,[54] but these results do not rule out the contribution of nonelectrostatic effects to the binding of other metal ions such as Mn^{2+} at higher salt concentrations. The direct structural data reported in this paper yield five aqua ligands and a single RNA-derived nitrogen ligand for Mn(II) in the presence of a slight excess of $tRNA^{Phe}$, a plausible structure for a unique site at high fractional occupancy. This result is consistent with the original interpretation of Leroy and Guéron that the tight sites observed at high salt do indeed involve specific binding, unlike the spectrum of sites observed at lower salt.[45] Structural information derived from pulsed EPR and binding curves derived by other means can each aid in the interpretation of the other and give rise to a coherent unified interpretation.

(52) Shi, H.; Moore, P. B. *RNA* **2000**, *6*, 1091−1105.
(53) (a) Walters, J. A. L. I.; Geerdes, H. A. M.; Hilbers, C. W. *Biophys. Chem.* **1977**, *7*, 147−151. (b) Guéron, M.; Leroy, J. L. *Biophys. J.* **1982**, *38*, 231−236.

Conclusions

Divalent metal ions are of central importance to the structure and function of many ribozymes and other nucleic acid systems. Nevertheless, structural techniques to analyze the ligation and surroundings of such ions in solution are quite limited. In this paper, we have demonstrated the utility of the pulsed EPR techniques of ESEEM and ESE-ENDOR to provide site-specific, complete, and highly precise characterization of the structural features of metal ions bound to nucleotides and nucleic acids. Although this paper has concentrated on a mononucleotide model system, data on yeast $tRNA^{Phe}$ and the hammerhead ribozyme provide assurance that generalization of the spectroscopic techniques to larger systems will be straightforward. For any particular structured RNA of interest, the main obstacle to overcome will be the separation of the specific ion interactions of interest from the large number of background, nonspecific potential metal-binding sites. As seen here for tRNA and the hammerhead ribozyme, the careful choice of monovalent salt conditions is critical for this distinction. We anticipate that the combination of techniques demonstrated in this paper will allow substantial new insights into the structural mechanisms by which divalent metal ions play their diverse roles in ribozymes and other functional nucleic acids.

Acknowledgment. This work was supported by NIH grant GM61211 to R.D.B. The authors are grateful to Jeffrey Peloquin and Kris Campbell for assistance with data acquisition and interpretation, to David Randall for coding the ESE-ENDOR simulation routine and for helpful discussions, and to Thorsten Dieckmann and his laboratory for the gift of isotopically labeled GMP.

Supporting Information Available: Details on ligation site identification in MnGMP using deuterium labeling and on quantitation of the hydration of Mn(II) ligated to GMP (PDF). This material is available free of charge via the Internet at http://pubs.acs.org.

JA0112238

(54) Misra, V. K.; Draper, D. E. *J. Mol. Biol.* **2000**, *299*, 813−825.